Supplementary Information

Mass spectrometry

Negative ion MALDI mass spectra of $C_{76}(CF_3)_nF_m$ were acquired using a reflector time-of-flight Bruker AutoFlex II mass spectrometer (N_2 laser, 337 *nm*, 2.5 *ns* pulse). *Trans*-2-[3-(4-*tert*-butylphenyl)-2-methyl-2-propenylidene]malonodinitrile (DCTB, ≥98%, Sigma-Aldrich) was used as a matrix; matrix-to-analyte molar ratio exceeded 1000. MALDI mass spectrum of sublimated trifluoromethylation product is shown in Figure S1, in which a more detailed assignment of spectral peaks is given as compared with Figure 1 of the main text.

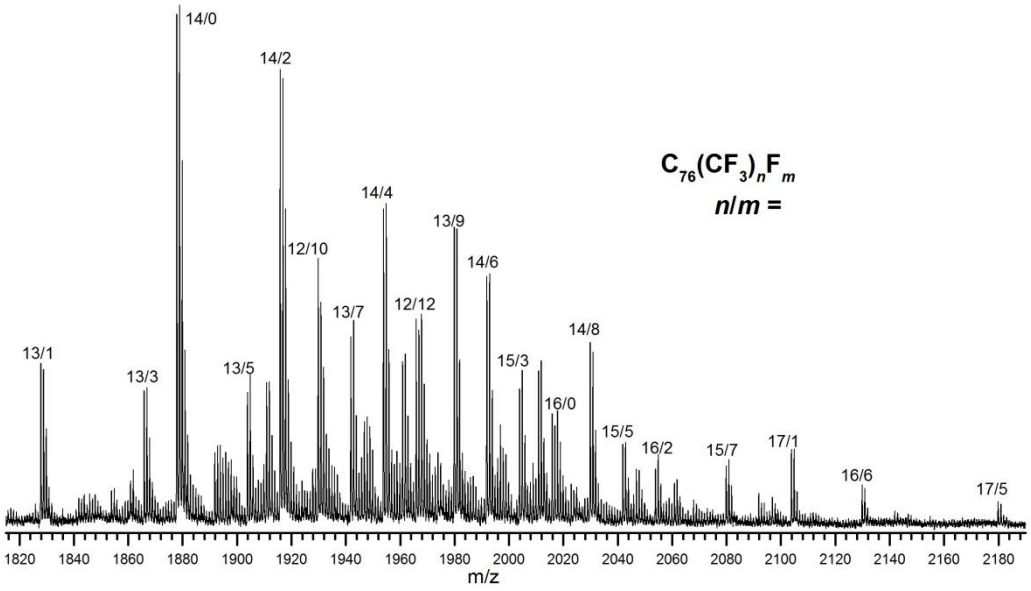

Figure S1. Negative ion MALDI mass spectra of the trifluormethylation product with compositions $C_{76}(CF_3)_nF_m$ denoted as *n*/*m*.

Chromatographic isolation of $C_{76}(CF_3)_nF_m$ fractions

The trifluoromethylation product was dissolved in toluene and subjected to HPLC separation in toluene using a preparative Buckyprep column (20 i.d. × 250 mm, Nacalai Tesque Inc.) and a flow rate of 18 mL min^{-1}. HPLC trace in the range of 5 – 45 min is shown in Figure S2. Inset in Figure S2 shows an enlarged part of the chromatogram in the range of 8 – 21 min and time intervals of the collection of three fractions subjected to additional separation.

Details of the additional purification of fractions p7, p9, and p10 in toluene using a semi-preparative Buckyprep column (10 i.d. × 250 mm, Nacalai Tesque Inc.) and a flow rate of 4.6 mL min^{-1} are presented in Figure S3. Subfractions p7-2, p9-2, and p10-2 gave small crystals by slow evaporation of toluene or recrystallization from *p*-xylene.

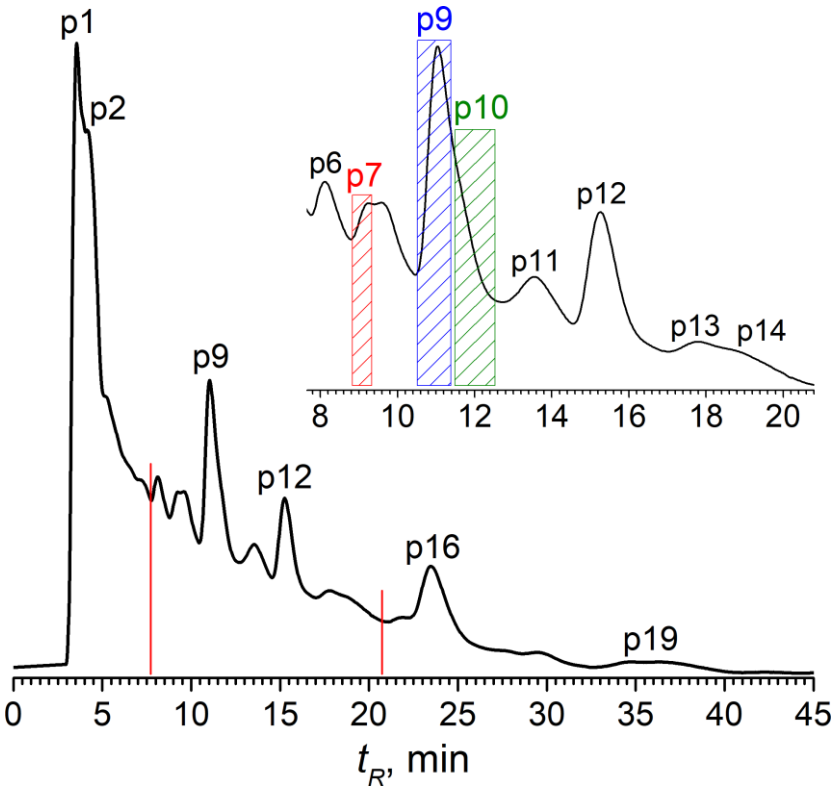

Figure S2. HPLC separation (Cosmosil Buckyprep, 20 mm I.D. x 25 cm, toluene, 18 mL·min^{-1}) of the trifluoromethylation product.

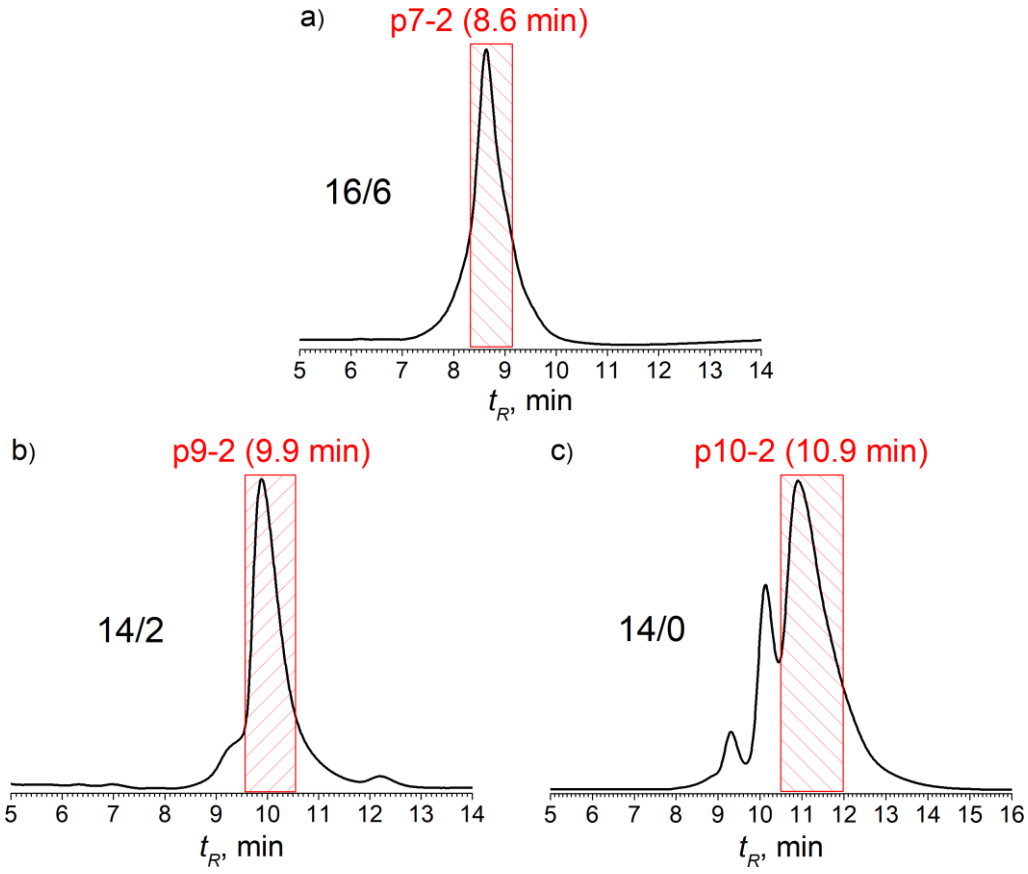

Figure S3. HPLC isolation (Cosmosil Buckyprep, 10 mm I.D. x 25 cm, toluene, 4.6 mL·min^{-1}) of the fractions obtained in the first separation step. Fractions p7-2 (a), p9-2 (b), and p10-2 (c) gave crystals of non-IPR $C_{76}(CF_3)_nF_m$ with *n*/*m* 16/6, 14/2, and 14/0, respectively.

X-ray crystallography

Synchrotron X-ray data were collected at 100 K on BL14.3 and BL14.2 at the BESSY storage ring (Berlin, Germany) using a MAR225 detector (λ = 0.8950 Å) or a pixel detector PILATUS (λ = 0.8266 Å). All structures were solved and anisotropically refined using the SHELX package. Selected crystallographic data and CCDC deposition numbers are given in Table S1.

Table S1. Selected crystallographic data and some details of data collection and refinement for $C_{76}(CF_3)_nF_m$.

Compound	**$C_{76}(CF_3)_{14}$**	**$C_{76}(CF_3)_{14}$**	**$C_{76}(CF_3)_{14}F_2$**	**$C_{76}(CF_3)_{14}F_2$**	**$C_{76}(CF_3)_{16}F_6$**
Solvate molecule	2 PhMe	–	–	1.4 PhMe	2 *p*-xylene
M_r	2063.17	1878.90	1916.90	2045.89	2343.24
crystal system	triclinic	monoclinic	triclinic	triclinic	monoclinic
space group	$P\ \bar{1}$	$P2_1/c$	$P\ \bar{1}$	$P\ \bar{1}$	$P2_1/n$
a [Å]	12.5151(5)	22.473(2)	10.060(1)	12.586(1)	21.606(2)
b [Å]	15.2489(8)	9.962(1)	14.746(1)	15.281(1)	15.048(1)
c [Å]	21.0810(7)	28.182(3)	22.431(2)	21.008(2)	24.002(2)
α [°]	103.081(2)	90	107.86(1)	103.460(6)	90
β [°]	98.872(4)	107.717(10)	91.90(1)	99.610(8)	95.32(1)
γ [°]	106.795(5)	90	105.28(1)	107.79(1)	90
V [Å^3]	3646.0(3)	6010.0(11)	3031.6(5)	3615.8(6)	7770.1(11)
Z	2	4	2	2	4
D_c [g cm^{-3}]	1.879	2.077	2.100	1.879	2.003
refls collected /R_{int}	55923/0.043	83046/0.194	45913/0.211	54426/0.151	102462/0.106
data / parameters	14461 /1371	13011 /1189	12100 /1226	14181/1382	21052 /1463
$R_1(I \geq 2\sigma(I))$ /wR_2(all)	0.059/ 0.148	0.107/0.273	0.139/0.341	0.134/0.296	0.065/0.142
$\Delta\rho_{max / min}$ [e Å^{-3}]	1.00 /–0.49	0.47 / -0.48	0.62 /–0.51	0.59 /–0.49	0.87 / -0.41
CCDC	**1812768**	**1812769**	**1812770**	**1812771**	**1812772**

Taking into account similar unit cell dimensions and symmetry of structures $C_{76}(CF_3)_{14}$ (CCDC 1812768) and $C_{76}(CF_3)_{14}F_2$ (CCDC 1812771) they seem to be nearly isomorphous though the compositions are different. We suppose this to be due to the similarity of the main molecules because two F atoms (distributed over four sites) do not change the overall shape of the molecule (the positions of CF_3 groups define the shape). Small changes in the amount of toluene molecules contained in the crystal packing (1.4 vs. 2.0) is reflected in the smaller unit cell volume of structure $C_{76}(CF_3)_{14}F_2$ (CCDC 1812771).

In both crystal structures of $C_{76}(CF_3)_{14}F_2$ and $C_{76}(CF_3)_{14}F_2 \cdot 1.5$ PhMe, two F atoms attached to C_{76} carbon cage are disordered over four positions. In both structures, the refined occupation ratio of two pairs of F atoms on both sides of $C_{76}(CF_3)_{14}F_2$ molecules has roughly the same value of 61/39.

Small disorder is present in the structure of $C_{76}(CF_3)_{16}F_6$ which can be interpreted as possible interchange of positions of a CF_3 group and a neighboring F atom. This disorder type has been neglected in the structure description.

Pathways of cage transformations in IPR C_{76}(1)

A topological search for all possible shortest pathways from D_2-C_{76} ($^{\#19150}C_{76}$) to non-IPR C_{76}(*NC*2) found experimentally in the molecular structures was carried out by using a local computer program. It was established that five Stone-Wales rearrangements (SWRs) are necessary which are interchangeable. It means that separate rotations of C–C bonds can proceed in any order thus giving altogether 120 (5!) pathways. However, some of them are identical due to D_2-symmetry of the starting C_{76} cage and C_2 symmetry of the final one, giving 50 different pathways. The choice of the most probable pathway is arbitrary from topological point of view. A similar topological analysis of cage transformations from D_2-C_{76} to non-IPR C_{76} cages, $^{\#18387}C_{76}$ and $^{\#18917}C_{76}$, found previously, suggests four and seven SWRs, respectively.[S1,S2]

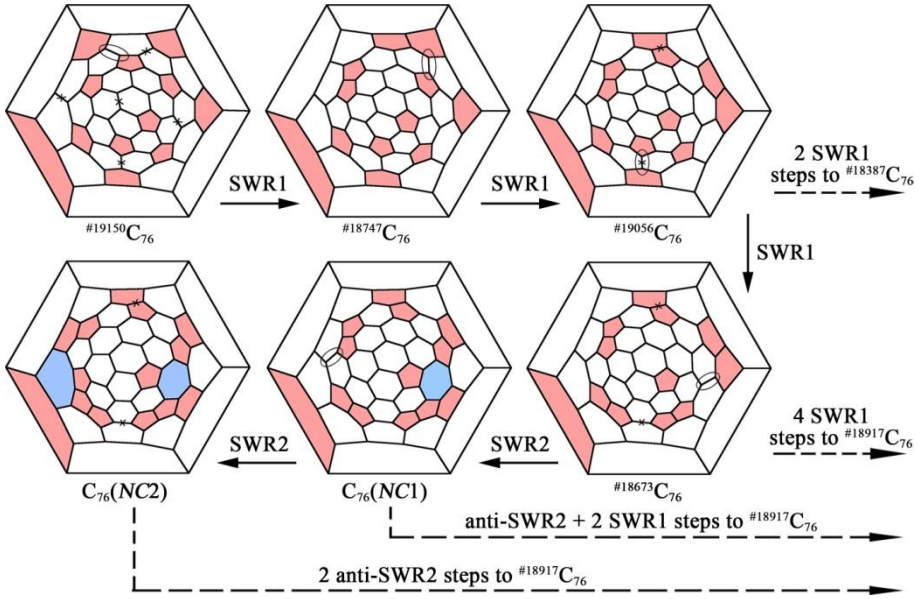

Figure S4. Probable pathways of cage transformations of D_2-C_{76} ($^{\#19150}C_{76}$).

The pathways shown in Figure S4 and in Figure 4 of the main text is based on the finding that three different pathways, to C_{76}(*NC*2), $^{\#18387}C_{76}$, and $^{\#18917}C_{76}$, may possess common steps, i.e. they can be included into a general, branched transformation scheme. The scheme on Figure S4 demonstrates that the pathways from IPR $^{\#19150}C_{76}$ to non-IPR C_{76}(*NC*2) and non-IPR $^{\#18387}C_{76}$ can possess two common steps whereas three common steps are possible on pathways from IPR $^{\#19150}C_{76}$ to non-IPR C_{76}(*NC*2) and non-IPR $^{\#18917}C_{76}$. Noteworthy, the pathway to non-IPR C_{76}(*NC*2), which contains two cage heptagons, should include two Stone-Wales rearrangements of the type SWR2 whereas two other final non-IPR cages, $^{\#18387}C_{76}$, and $^{\#18917}C_{76}$, can be achieved by exclusively SWR1 steps . At the same time, a pathway $^{\#18917}C_{76}$ may include SWR2 as well (for classification of SWRs see ref. S3). In particular, heptagons created on 4th and 5th steps of the pathway shown by Schlegel diagrams in Figure S4 can be eliminated, thus resulting in classical, non-IPR $^{\#18917}C_{76}$. However, such transformation routes demand passing a SWR of a new type, anti-SWR2, which starts from a patch consisting of two opposite pentagons, one

hexagon, and one heptagon and results in a patch consisting of one pentagon and three hexagons. However, a feasibility of anti-SWRs in chlorination-promoted cage transformations is so far confirmed neither experimentally nor theoretically.

References

S1 a) I. N. Ioffe, A. A. Goryunkov, N. B. Tamm, L. N. Sidorov, E. Kemnitz, S. I. Troyanov, *Angew. Chem., Int. Ed.* 2009, **48**, 5904; b) I. N. Ioffe, O. N. Mazaleva, C. Chen, S. Yang, E. Kemnitz, S. I. Troyanov, *Dalton Trans*. 2011, **40**, 11005.

S2 S. M. Sudarkova, O. N. Mazaleva, R. A. Konoplev-Esgenburg, S. I. Troyanov, I. N. Ioffe, *Dalton Trans.* 2018, **47**, 4554.

S3 I. N. Ioffe, S. Yang, S. Wang, E. Kemnitz, L. N. Sidorov, S. I. Troyanov, *Chem. – Eur. J*. 2015, **21**, 4904.